

Asymptotic freedom, lost: Complex conformal field theory in the two-dimensional $O(N > 2)$ nonlinear sigma model and its realization in the spin-1 Heisenberg chain

Christopher Yang¹ and Thomas Scaffidi¹

¹*Department of Physics and Astronomy, University of California, Irvine, Irvine, California 92697, USA*

The two-dimensional $O(N)$ nonlinear sigma model (NLSM) is asymptotically free for $N > 2$: it exhibits neither a nontrivial fixed point nor spontaneous symmetry-breaking. Here we show that a nontrivial fixed point generically does exist in the *complex* coupling plane and is described by a complex conformal field theory (CCFT). This CCFT fixed point is generic in the sense that it has a single relevant singlet operator, and is thus expected to arise in any non-Hermitian model with $O(N)$ symmetry upon tuning a single complex parameter. We confirm this prediction numerically by locating the CCFT at $N = 3$ in a non-Hermitian spin-1 antiferromagnetic Heisenberg chain, finding good agreement between the complex central charge and scaling dimensions and those obtained by analytic continuation of real fixed points from $N \leq 2$. We further construct a realistic Lindbladian for a spin-1 chain whose no-click dynamics are governed by the non-Hermitian Hamiltonian realizing the CCFT. Since the CCFT vacuum is the eigenstate with the smallest decay rate, the system naturally relaxes under dissipative dynamics toward a CFT state, thus providing a route to preparing long-range entangled states through engineered dissipation.

Introduction.—The $O(N)$ nonlinear σ -model (NLSM) occupies a central role in quantum field theory and describes a diverse class of systems, such as magnetic systems, superfluids, and chiral effective models in quantum chromodynamics [1–10]. In two dimensions, it famously flows to strong coupling in the infrared for $N > 2$, the simplest example of asymptotic freedom. This results in the absence of an ordered phase and of a non-trivial fixed point at finite coupling [2, 4, 11–15]. These properties reflect the Mermin-Wagner theorem, which forbids the spontaneous breaking of continuous symmetries in 2D [16], and seem to preclude any nontrivial fixed point.

In this work, we show that this conclusion can be dramatically altered in non-Hermitian settings—relevant, for example, to monitored quantum dynamics—where in the field-theory formulation the only change is that the coupling becomes complex, $g \in \mathbb{C}$, in the $O(N)$ NLSM:

$$S = \frac{1}{2g} \int d^2x (\nabla \hat{n})^2. \quad (1)$$

Here \hat{n} is an N -component unit vector, $\hat{n} \in S^{N-1}$.

As we will show, allowing g to be complex reveals a pair of complex conjugate fixed points described by a complex conformal field theory (CCFT) [17–23] with a complex central charge $c(N) \in \mathbb{C}$, e.g. $c \approx 1.51 \pm 0.158i$ for $O(3)$ (see Eq. (2) for the general expression of $c(N)$). This complex fixed point gives rise to a spiral Renormalization Group (RG) flow in the complex plane for g , schematically shown in Fig. 1. Asymptotic freedom is thus generically lost in the non-Hermitian version of the NLSM because there is now a large part of the phase diagram which in the UV flows to the non-Gaussian CCFT, rather than the trivial $g = 0$ fixed point.

Complex CFTs describe fixed points which have moved to the complex plane through the annihilation of two real fixed points, and have been proposed as a natural explanation for the conformality loss and the “walking

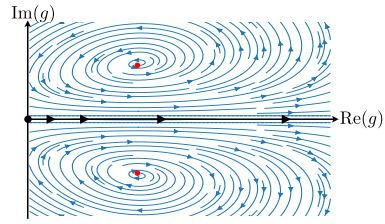


FIG. 1. Schematic RG flow (from UV to IR) of the 2D $O(N > 2)$ nonlinear σ -model (NLSM) with a complex coupling parameter g . On the real axis, the flow goes to strong coupling. The CCFTs (red dots) appear at complex-conjugate positions in the complex- g plane, around which the flow forms an outward spiral which eventually also flows to strong coupling.

behavior” (or weakly first-order transitions) observed on the real axis of a variety of condensed matter and high-energy systems [17, 18, 20, 24–35]. Subsequently, numerical works studied complex fixed points directly by working with non-Hermitian Hamiltonians or transfer matrices in a variety of models, including the $Q > 4$ Potts models [23, 35–39] and $O(N > 2)$ loop models [22], which are closely related to the fixed points described here, as we will explain. (See also recent works on quantum spin models [40, 41]). However, two critical questions remain: (1) How generic are CCFTs—can they be found in a broad class of systems? and (2) Can they be realized in an experimentally relevant non-Hermitian system?

We address these questions as follows. First, we show that the $O(N)$ complex fixed points introduced here are generic: they possess a single relevant singlet operator with $\text{Re}(\Delta_\epsilon) < 2$, and thus emerge by tuning a single *complex* parameter. They are therefore expected in any non-Hermitian system with $O(N)$ symmetry, for $N > 2$.

Second, to address physical realization we propose a simple microscopic model—the non-hermitian spin-1 Heisenberg chain—which realizes the $O(3)$ CCFT fixed

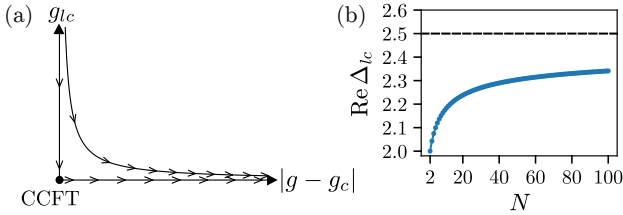


FIG. 2. (a) Schematic two-parameter RG flow for the $O(N > 2)$ NLSM. The parameter $|g - g_c|$ is the distance from the critical point g_c in the complex plane of the coupling constant g , and thus corresponds to the energy operator ϵ , which is relevant. The parameter g_{lc} controls the strength of the “loop crossings” and corresponds to the 4-leg watermelon operator, with scaling dimension $\Delta_{lc} \equiv \Delta_{l=4}$, which is irrelevant at the CCFT. Contrary to the loop model, for which $g_{lc} = 0$ due to an additional microscopic, non-invertible symmetry, the NLSM generically has $g_{lc} \neq 0$ in the UV. It therefore only flows toward $g_{lc} = 0$ in the IR, realizing the same non-invertible symmetry as the loop model, but now as an *emergent* symmetry that appears only at the CCFT fixed point. (b) Scaling dimension of loop crossings Δ_{lc} , which are irrelevant for all $N > 2$. The dashed line indicates the asymptote $\text{Re } \Delta_{lc}(N \rightarrow \infty) = 2.5$.

point. We confirm our results non-perturbatively by locating this fixed point via exact diagonalization of the non-Hermitian Hamiltonian. Using operator-state correspondence to map the low-lying spectrum $\epsilon_\mu - i\gamma_\mu$ of this Hamiltonian to CFT operators, we find close agreement with predicted scaling dimensions. The eigenstate corresponding to the CCFT vacuum exhibits not only the lowest energy ϵ_μ but also the slowest decay rate γ_μ . Consequently, time evolution under this Hamiltonian naturally relaxes the system to the CCFT vacuum state. Finally, we provide a microscopic Lindbladian for a spin-1 chain whose no-click dynamics (accessible via continuous monitoring and post-processing, see e.g. Ref. [42]) realizes this non-Hermitian Hamiltonian.

From an open quantum dynamics perspective, our work establishes CCFTs as a new universality class to describe criticality in dissipative quantum systems [43–51], and provides a distinct example of how dissipation can induce a unique form of criticality that is otherwise impossible in equilibrium. The CCFT we identify has a complex central charge and is thus distinct from several critical phases previously studied in non-Hermitian systems. In particular, it cannot be obtained by a complex deformation of a unitary CFT [47], nor is it equivalent to a non-unitary CFT with negative but real central charge, as has been predicted in a number of non-Hermitian settings [52–57]. In the context of monitored dynamics and quantum state preparation [54, 58–62], our work introduces a route to prepare highly-entangled critical phases with universal properties. The complex fixed point we find has logarithmic entanglement scaling with a universal central charge, contrasting with the non-universal ef-

fective central charges previously found to govern some dissipation-induced entanglement transitions [63–68].

O(N) loop model.— The $O(N)$ CCFTs we investigate appear naturally in the context of $O(N)$ loop models [69–76]. There, they are the analytic continuation to $N > 2$ of two branches of real fixed points which annihilate at $N = 2$ and move to the complex plane for $N > 2$. (In the $O(N)$ loop model, N is a continuous parameter giving the loop fugacity [22]). Using Coulomb gas methods, these loop models were shown to have central charge

$$c_\pm(N) = 1 - \frac{6(1 - \tilde{g}_\pm)^2}{\tilde{g}_\pm}, \quad (2)$$

where $\tilde{g}_\pm = 1 \pm e(N)$ and $e(N) = \frac{1}{\pi} \cos^{-1}(N/2)$ [22, 70–76]. For $N < 2$, these two branches correspond to two different real CFTs, describing the dense and dilute phases of $O(N)$ loop models (e.g. for $N = 1$ the dilute phase describes the Ising CFT). For $N > 2$, $e(N)$ becomes purely imaginary, and the two branches form a complex conjugate pair of CCFTs with complex central charge [22].

The scaling dimensions also become complex for $N > 2$, and can similarly be predicted by analytic continuation of the $O(N \leq 2)$ results [22, 75]. In particular, the thermal scaling dimension, associated with the loop tension in the loop model and to the energy operator in the NLSM, is given by

$$\Delta_\epsilon = 4/\tilde{g}_\pm - 2. \quad (3)$$

Another set of operators are the ℓ -leg watermelon operators [74], which in the loop model correspond to having ℓ loop strands emanating from or terminating at a point. They have scaling dimension

$$\Delta_\ell = \frac{1}{8} \tilde{g}_\pm \ell^2 - \frac{(1 - \tilde{g}_\pm)^2}{2\tilde{g}_\pm}. \quad (4)$$

For instance, the $\ell = 1$ watermelon operator corresponds to the $O(N)$ vector field \hat{n} and $\Delta_{\ell=1}$ thus governs the power-law decay of the two-point function between $O(N)$ spins [74]. More generally, the multiplicity of watermelon operators for $\ell > 1$ appears as the *sum* of distinct $O(n)$ irreducible representations, and this was recently explained by the presence of an additional, non-invertible symmetry (associated with topological defect lines) [77–79] present at the microscopic level in the loop model.

Predictions for the $O(N)$ NLSM.— We now discuss how to port these results from the loop models to the NLSM. What differentiates the two models is that the NLSM allows for “loop crossings” [80]. Indeed, $O(N)$ loop models arise as a truncated high-temperature expansion of the $O(N)$ classical Heisenberg model, where the truncation amounts to neglecting loop crossings [69]. If loop crossings are relevant, the loop model and the NLSM are in different universality classes. (This is what happens on the dense branch for $N < 2$ [80].) Conversely, if

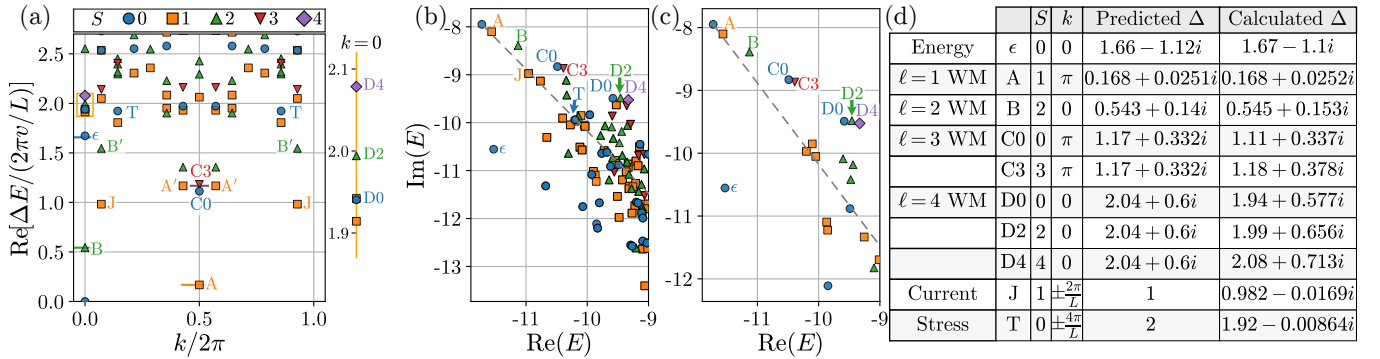


FIG. 3. Spectrum of the Heisenberg spin-1 chain at the finite-size complex fixed point [Eq. (6)] for a length $L = 14$ chain. (a) Real part of the extracted scaling dimensions, obtained as rescaled energy gaps $\Delta E/(2\pi v/L)$, where $\Delta E = E - E_g$ and E_g is the ground state energy and $v = 0.796 - 1.03i$ is the complex velocity. Different colors and symbols indicate states with distinct $O(3)$ total spin number S . Letters label states with known $O(N)$ CCFT predictions, as summarized in panel (d). Narrow horizontal lines denote the predicted real parts of the scaling dimensions. States labeled by primed letters correspond to descendants of the primaries labeled by the corresponding unprimed letters. On the right, we zoom in on the orange box enclosing states at $k = 0$ with nearly-marginal scaling dimensions, of which $D0$, $D2$, and $D4$ arise from the $\ell = 4$ watermelon operator. (b) Energy spectrum in the complex plane without rescaling by $2\pi v/L$, with the dashed line parameterized by $E_g + vx$, where $x \in \mathbb{R}^+$ showing the direction of the conformal towers. Note that we shift the eigenenergies by an imaginary constant δ (see the discussion following Eq. (8)). (c) Same as (b), but only displaying states with momenta $k = 0$ and π . On this panel, the clusters of nearly-degenerate states corresponding to the $\ell = 1, 2, 3, 4$ watermelon operators (labeled by A, B, C, D) become obvious. (d) Table of identified CCFT states, comparing the predicted and numerically calculated scaling dimensions Δ . WM stands for watermelon operators.

loop crossings are irrelevant, the loop model fixed points should also describe the generic critical behavior of the NLSM (See Fig. 2a). Crucially, this is what happens for $N > 2$: loop crossings, which correspond to the singlet component of the $\ell = 4$ watermelon operators [80], are irrelevant for $N > 2$ (see Fig. 2b). The loop model $O(N)$ CCFT fixed points therefore describe the generic criticality of the non-Hermitian $O(N)$ NLSM as well. As a side result, it also means that the non-invertible symmetry of loop models introduced in Ref. [79] is expected to appear for the NLSM as well, but as an *emergent* symmetry at the CCFT fixed point.

Microscopic model and numerical results.— As a concrete example at $N = 3$ with experimental relevance to quasi-1D antiferromagnets [81, 82] and various quantum simulator platforms [83, 84], we study the spin-1 Heisenberg chain described by the Hamiltonian [85]

$$H = \sum_i \left[J_1 \mathbf{S}_i \cdot \mathbf{S}_{i+1} + J_2 \mathbf{S}_i \cdot \mathbf{S}_{i+2} + K (\mathbf{S}_i \cdot \mathbf{S}_{i+1})^2 \right], \quad (5)$$

where $\mathbf{S}_i = (S_i^x, S_i^y, S_i^z)$ represents the vector of spin-1 matrices S_i^α acting on site i , with $\alpha = x, y, z$. Here, J_1 , J_2 , and K denote the coupling parameters for nearest-neighbor exchange, second neighbor exchange, and nearest-neighbor biquadratic coupling, which are the three simplest local $SU(2)$ -symmetric terms, with J_1 being typically the largest term (we will take $J_1 = 1$).

As long as J_2 and K are not too large compared to J_1 , this Hamiltonian realizes a gapped, short-range entangled, paramagnetic phase with symmetry-protected

topological order called the Haldane phase. This phase is well described by the $O(3)$ NLSM of Eq. (1) with a coupling constant g that depends on J_2 and K , see Refs. [11, 13, 15, 86]. The flow to strong coupling of the NLSM on the real axis explains the absence of antiferromagnetic order, the finite gap, and the exponentially decaying correlations in the spin-1 Heisenberg chain [11]. By allowing J_2 and K to be complex, however, we will obtain an NLSM with a complex coupling constant $g(J_2, K) \in \mathbb{C}$ which exhibits a critical fixed point at $g = g_c$ described by a CCFT with power-law correlations.

Before moving on to the numerical results, we address a practical challenge in the numerics. As shown in Fig. 2(a), accessing the CCFTs should require the tuning of a single complex parameter, since there is a single relevant singlet operator ϵ . However, the loop crossing operator, which is the singlet component of the $\ell = 4$ watermelon operator, is only weakly irrelevant for $N = 3$: it has scaling dimension $\text{Re} \Delta_{\ell=4} \approx 2.04$, as shown in Fig. 2(b). This means the loop crossing coupling constant g_{lc} decays very weakly with system size as $\sim L^{-0.04}$, which leads to very slow finite size convergence to the CCFT fixed point in our numerics. To address this issue, we decide to tune an additional parameter which allows us minimize the loop crossing strength g_{lc} in the Hamiltonian, thus leading to much faster finite size convergence to the CCFT fixed point. (That would be less of an issue at larger N since the loop crossing operator becomes more irrelevant as N increases, although it does so slowly, see Fig. 2(b).)

Using exact diagonalization on a periodic chain of length $L = 14$, and a gradient descent method to find the location of a finite-size critical point with optimal finite size convergence, we find a complex conjugate pair of critical points at

$$(J_2, K)_\pm = (0.0660 \pm 0.338i, 0.176 \pm 0.335i). \quad (6)$$

We focus on the point $(J_2, K)_+$ in the rest of the Letter, which realizes the c_+ branch in Eq. (2). At that point, the low-energy spectrum, see Fig. 3, displays primary and descendant states in close agreement with the CCFT predictions. Specifically, Fig. 3(a) shows the finite-size estimates of the scaling dimensions, calculated as rescaled energy gaps $\Delta E/(2\pi\nu/L)$, with $\Delta E = E - E_g$ [87]. The ground state, with energy E_g , is defined as the eigenvalue with the smallest real part [88]. The value of the velocity was obtained numerically $v = 0.796 - 1.03i$ (see End Matter). As expected for a critical state, the entanglement of the ground state grows logarithmically with subsystem size, and the extracted central charge agrees well with the prediction: $c = 1.529 - 0.161i$ within 2% of the predicted value $c_+ = 1.51 - 0.158i$ (see End Matter for more details).

Identification of CFT operators.— Each eigenstate has a well-defined lattice momentum k and $O(3)$ spin quantum number S . The first singlet ($S = 0$) excited state in the $k = 0$ sector is identified with ϵ , the energy operator of the NLSM. The corresponding scaling dimension governs the spiral flow of g around the fixed point, according to $g - g_c \sim L^{2-\Delta_\epsilon}$. We find a good agreement between the Coulomb gas prediction $\Delta_\epsilon \approx 1.66 - 1.12i$ and our numerically obtained value of $1.67 - 1.1i$. We also find good agreement for the stress tensor, labeled T , with predicted scaling dimension $\Delta_T = 2$ at $S = 0$ and $k = \pm 4\pi/L$, and the $O(N)$ current, labeled J , with predicted scaling dimension $\Delta_J = 1$ at $S = 1$ and $k = \pm 2\pi/L$ (see Fig. 3(d)).

The ℓ -leg watermelon operators appear in the spectrum as clusters of nearly-degenerate states with different S values, at momentum $k = 0$ for even ℓ and momentum $k = \pi$ for odd ℓ (see Fig. 3(c) where the clusters are labeled by A,B,C,D for $\ell = 1, 2, 3, 4$). As explained in the End Matter, we find a perfect matching between the predicted decomposition of ℓ -leg watermelon operators into $O(n)$ irreducible representations [78] and the clusters of nearly-degenerate spin multiplets we observe in our spectrum. This approximate degeneracy between distinct spin multiplets arises due to the emergent non-invertible symmetry mentioned above [79], and should thus become exact in the thermodynamic limit.

Realization with monitored quantum dynamics.— Since we have found a CCFT fixed point in a simple microscopic non-Hermitian Hamiltonian (NHH) H , it now makes sense to ask whether it could be realized in quantum dynamics. Time evolution with a NHH can be realized by continuous monitoring and post-processing to select only trajectories with no clicks [89–91]. In that

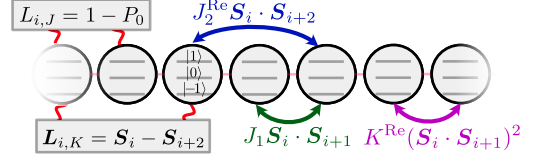


FIG. 4. Realization of a CCFT in a spin-1 Heisenberg chain. Non-Hermiticity can be engineered by introducing jump operators $S_i - S_{i+2}$ and $1 - P_0$, where $P_0 = (1/3)[(S_i \cdot S_{i+1})^2 - 1]$ is a projector onto the singlet sector. After post-selection on no-click trajectories, the dynamics are governed by a non-Hermitian Hamiltonian with a complex J_2 and K , which can be tuned to a CCFT.

case, up to a normalization, the dynamics is described by $|\psi(t)\rangle = e^{-iHt}|\psi(0)\rangle$. Denoting the right eigendecomposition of H as

$$H|\psi_{R,\mu}\rangle = (\epsilon_\mu - i\gamma_\mu)|\psi_{R,\mu}\rangle, \quad (7)$$

we identify from the spectrum frequencies $\epsilon_\mu \in \mathbb{R}$ and decay rates $\gamma_\mu \in \mathbb{R}_+$.

As shown in Fig. 3(b), the state corresponding to the CFT vacuum $|\psi_{\text{CFT}}\rangle$ is not only the ground state (i.e., with lowest energy ϵ), but it is also the “longest-lived state” LLS (i.e., with lowest decay rate γ). Any initial state with a non-zero overlap with the LLS will asymptotically approach it at late times, and thus we have $|\psi(t \rightarrow \infty)\rangle \propto |\psi_{\text{CFT}}\rangle$. This shows that dissipation naturally drives the system into the CCFT, and thus provides a way of preparing a highly non-trivial, long-range entangled CFT ground state through engineered dissipation. More generally, e^{-iHt} is guaranteed to relax the system towards a CFT primary state so long as the velocity has negative imaginary part ($\text{Im}(v) < 0$). Indeed, in that case the primary operator is necessarily the longest-lived state within its conformal family since descendants have decay rates which increase in increments of $(2\pi|\text{Im}(v)|)/L$ (see Fig. 3(b)).

We now give an explicit Lindblad master equation whose no-clicks trajectories realizes the non-Hermitian spin-1 Heisenberg chain of Eq. (5). The open system is modeled by a density matrix ρ that obeys the Lindblad master equation

$$\partial_t \rho = -i[H_0, \rho] - \sum_a (L_a \rho L_a^\dagger - \frac{1}{2}\{L_a^\dagger L_a, \rho\}), \quad (8)$$

where H_0 is the Hermitian Hamiltonian of the closed system and L_a are the jump operators that describe coupling to the environment. When postselecting for no-click trajectories, the system evolves under an effective non-Hermitian Hamiltonian $H_{\text{eff}} = H_0 - \frac{i}{2}\sum_a L_a^\dagger L_a$ [89–91]. Here, we choose for the closed system Hamiltonian

$$H_0 = \sum_i [J_1 S_i \cdot S_{i+1} + J_2^{\text{Re}} S_i \cdot S_{i+2} + K^{\text{Re}} (S_i \cdot S_{i+1})^2], \quad (9)$$

and engineer the imaginary terms for J_2 and K via the jump operators $L_{i,J} = \sqrt{J_2^{\text{Im}}}(\mathbf{S}_i - \mathbf{S}_{i+2})$ and $L_{i,K} = \sqrt{6K^{\text{Im}}}(1 - P_0)$, where $i = 1, \dots, L$ and $P_0 = (1/3)[(\mathbf{S}_i \cdot \mathbf{S}_{i+1})^2 - 1]$ is the projector onto the singlet sector. The resulting H_{eff} realizes the same Hamiltonian we studied numerically (Eq. (5)) with $J_2 = J_2^{\text{Re}} + iJ_2^{\text{Im}}$ and $K = K^{\text{Re}} + iK^{\text{Im}}$. (There is also an additional constant imaginary shift $\delta \equiv -i(4K^{\text{Im}} + J_2^{\text{Im}})L$.)

Discussion.— We have established the existence of a critical fixed point of the 2D $O(N)$ NLSM for $N > 2$ at a complex value of the coupling g . An immediate implication is for perturbation theory: at any fixed loop order, a truncated beta function $\beta(g)$ must generically admit zeros away from the positive real axis. It would be interesting to assess whether these perturbative zeros align with the CCFT points identified here, providing a nontrivial consistency check on the perturbative expansion [92]. More broadly, whether these complex fixed points could influence the flow on the real axis in the NLSM remains to be determined [93].

Our microscopic analysis so far focused on the fixed point, but it would be valuable to map out the surrounding phase diagram. Based on the schematic flow in Fig. 1, one expectation is that the critical point manifests as an “unnecessary transition” *within* the Haldane phase, in the sense that all trajectories in its vicinity ultimately run to the same strong coupling fixed point. The situation could be richer, however, as in loop models where a CCFT describes the endpoint of a first-order line separating a “loop gas” from a “loop liquid” [22].

Finally, we proposed a protocol to prepare the CCFT ground state from generic initial states via continuous monitoring and postselection in a spin-1 Heisenberg chain. Our analysis so far has focused primarily on spectral properties of the corresponding non-Hermitian Hamiltonian; it would be interesting in future work to identify more directly accessible signatures of the CCFT under this dynamics, for example in correlation functions. Another especially tantalizing direction is to realize this exotic criticality directly at the master-equation level, without the need for postselection. We also note that alternative realizations of complex $O(N)$ nonlinear sigma models may be possible in monitored dynamics of free fermions [94].

We thank Slava Rychkov, Sagar Vijay, Ehud Altman, Kazuaki Takasan, Steven White, and Zlatko Papic for insightful discussions. This work was supported by the U.S. Department of Energy, Office of Science, Office of Basic Energy Sciences under Early Career Research Program Award Number DE-SC0025568. C.Y. gratefully acknowledges support from the Eddleman Quantum Institute postdoctoral fellowship.

- [1] J. M. Kosterlitz and D. J. Thouless, *Journal of Physics C: Solid State Physics* **6**, 1181 (1973).
- [2] A. Polyakov, *Physics Letters B* **59**, 79 (1975).
- [3] E. Brézin and J. Zinn-Justin, *Phys. Rev. Lett.* **36**, 691 (1976).
- [4] W. A. Bardeen, B. W. Lee, and R. E. Shrock, *Phys. Rev. D* **14**, 985 (1976).
- [5] E. Brézin and J. Zinn-Justin, *Phys. Rev. B* **14**, 3110 (1976).
- [6] E. Witten, *Nuclear Physics B* **223**, 422 (1983).
- [7] J. Gasser and H. Leutwyler, *Annals of Physics* **158**, 142 (1984).
- [8] D. H. Friedan, *Annals of Physics* **163**, 318 (1985).
- [9] K. Gawedzki and A. Kupiainen, *Communications in Mathematical Physics* **106**, 533 (1986).
- [10] P. K. Mitter and T. R. Ramadas, *Communications in Mathematical Physics* **122**, 575–596 (1989).
- [11] F. Haldane, *Physics Letters A* **93**, 464 (1983).
- [12] F. D. M. Haldane, *Phys. Rev. Lett.* **61**, 1029 (1988).
- [13] N. Chepiga, I. Affleck, and F. Mila, *Phys. Rev. B* **93**, 241108 (2016).
- [14] E. Fradkin, *Field Theories of Condensed Matter Physics* (Cambridge University Press, 2013).
- [15] J. H. Pixley, A. Shashi, and A. H. Nevidomskyy, *Phys. Rev. B* **90**, 214426 (2014).
- [16] N. D. Mermin and H. Wagner, *Phys. Rev. Lett.* **17**, 1133 (1966).
- [17] V. Gorbenko, S. Rychkov, and B. Zan, *Journal of High Energy Physics* **2018** (2018), 10.1007/jhep10(2018)108.
- [18] V. Gorbenko, S. Rychkov, and B. Zan, *SciPost Phys.* **5**, 050 (2018).
- [19] A. F. Faedo, C. Hoyos, D. Mateos, and J. G. Subils, *Phys. Rev. Lett.* **124**, 161601 (2020).
- [20] F. Benini, C. Iossa, and M. Serone, *Phys. Rev. Lett.* **124**, 051602 (2020).
- [21] A. F. Faedo, C. Hoyos, D. Mateos, and J. G. Subils, *Journal of High Energy Physics* **2021** (2021), 10.1007/jhep10(2021)246.
- [22] A. Haldar, O. Tavakol, H. Ma, and T. Scaffidi, *Phys. Rev. Lett.* **131**, 131601 (2023).
- [23] J. L. Jacobsen and K. J. Wiese, *Phys. Rev. Lett.* **133**, 077101 (2024).
- [24] M. Itakura, *Journal of the Physical Society of Japan* **72**, 74 (2003), <https://doi.org/10.1143/JPSJ.72.74>.
- [25] D. B. Kaplan, J.-W. Lee, D. T. Son, and M. A. Stephanov, *Phys. Rev. D* **80**, 125005 (2009).
- [26] A. Nahum, J. T. Chalker, P. Serna, M. Ortúñoz, and A. M. Somoza, *Phys. Rev. X* **5**, 041048 (2015).
- [27] C. Wang, A. Nahum, M. A. Metlitski, C. Xu, and T. Senthil, *Phys. Rev. X* **7**, 031051 (2017).
- [28] S. Iino, S. Morita, N. Kawashima, and A. W. Sandvik, *Journal of the Physical Society of Japan* **88**, 034006 (2019), <https://doi.org/10.7566/JPSJ.88.034006>.
- [29] P. Serna and A. Nahum, *Phys. Rev. B* **99**, 195110 (2019).
- [30] H. Ma and Y.-C. He, *Phys. Rev. B* **99**, 195130 (2019).
- [31] R. Ma and C. Wang, *Phys. Rev. B* **102**, 020407 (2020).
- [32] J. D’Emidio, A. A. Eberharter, and A. M. Läuchli, *SciPost Phys.* **15**, 061 (2023).
- [33] Z. Zhou, L. Hu, W. Zhu, and Y.-C. He, *Phys. Rev. X* **14**, 021044 (2024).

[34] Y. Tang, H. Ma, Q. Tang, Y.-C. He, and W. Zhu, *Phys. Rev. Lett.* **133**, 076504 (2024).

[35] V. V. Linden, B. De Vos, K. Vervoort, F. Verstraete, and A. Ueda, “Spiral renormalization group flow and universal entanglement spectrum of the non-hermitian 5-state potts model,” (2025).

[36] M. Nauenberg and D. J. Scalapino, *Phys. Rev. Lett.* **44**, 837 (1980).

[37] J. L. Cardy, M. Nauenberg, and D. J. Scalapino, *Phys. Rev. B* **22**, 2560 (1980).

[38] M. Fukugita and M. Okawa, *Phys. Rev. Lett.* **63**, 13 (1989).

[39] H. Shimizu and K. Kawabata, *Phys. Rev. B* **112**, 085112 (2025).

[40] X. Zou, S. Yin, Z.-X. Li, and H. Yao, “Unraveling deconfined quantum criticality in non-hermitian easy-plane j - q model,” (2025).

[41] S. Kumar, S. Pujari, and J. D’Emidio, “Pseudocriticality in antiferromagnetic spin chains,” (2025).

[42] S. Gopalakrishnan and M. J. Gullans, *Phys. Rev. Lett.* **126**, 170503 (2021).

[43] E. G. Dalla Torre, E. Demler, T. Giamarchi, and E. Altman, *Phys. Rev. B* **85**, 184302 (2012).

[44] L. M. Sieberer, S. D. Huber, E. Altman, and S. Diehl, *Phys. Rev. Lett.* **110**, 195301 (2013).

[45] L. M. Sieberer, M. Buchhold, and S. Diehl, *Reports on Progress in Physics* **79**, 096001 (2016).

[46] A. Bácsi, C. u. u. u. P. m. c. Moca, G. Zaránd, and B. Dóra, *Phys. Rev. Lett.* **125**, 266803 (2020).

[47] K. Yamamoto, M. Nakagawa, M. Tezuka, M. Ueda, and N. Kawakami, *Phys. Rev. B* **105**, 205125 (2022).

[48] S. J. Garratt, Z. Weinstein, and E. Altman, *Phys. Rev. X* **13**, 021026 (2023).

[49] S. Han, D. J. Schultz, and Y. B. Kim, *Phys. Rev. B* **107**, 235153 (2023).

[50] A. I. Lotkov, D. V. Kurlov, A. K. Fedorov, N. A. Nemkov, and V. Gritsev, *Phys. Rev. B* **108**, 064312 (2023).

[51] S. Murciano, P. Sala, Y. Liu, R. S. K. Mong, and J. Alicea, *Phys. Rev. X* **13**, 041042 (2023).

[52] O. A. Castro-Alvaredo and A. Fring, *Journal of Physics A: Mathematical and Theoretical* **42**, 465211 (2009).

[53] R. Couvreur, J. L. Jacobsen, and H. Saleur, *Phys. Rev. Lett.* **119**, 040601 (2017).

[54] X. Chen, Y. Li, M. P. A. Fisher, and A. Lucas, *Phys. Rev. Res.* **2**, 033017 (2020).

[55] Y.-T. Tu, Y.-C. Tzeng, and P.-Y. Chang, *SciPost Phys.* **12**, 194 (2022).

[56] J. Dengis, R. König, and F. Pastawski, *New Journal of Physics* **16**, 013023 (2014).

[57] X.-C. Zhou and K. Wang, “Universal non-hermitian flow in one-dimensional pt-symmetric quantum criticalities,” (2024), arXiv:2405.01640 [cond-mat.stat-mech].

[58] B. Lapierre, P. Pelliconi, S. Ryu, and J. Sonner, *Phys. Rev. B* **112**, 104322 (2025).

[59] A. Biella and M. Schiró, *Quantum* **5**, 528 (2021).

[60] B. Kraus, H. P. Büchler, S. Diehl, A. Kantian, A. Micheli, and P. Zoller, *Phys. Rev. A* **78**, 042307 (2008).

[61] H. Weimer, M. Müller, I. Lesanovsky, P. Zoller, and H. P. Büchler, *Nature Physics* **6**, 382–388 (2010).

[62] L. M. Sieberer, M. Buchhold, J. Marino, and S. Diehl, *Rev. Mod. Phys.* **97**, 025004 (2025).

[63] A. D’Abbruzzo, V. Alba, and D. Rossini, *Phys. Rev. B* **106**, 235149 (2022).

[64] X. Turkeshi, A. Biella, R. Fazio, M. Dalmonte, and M. Schiró, *Phys. Rev. B* **103**, 224210 (2021).

[65] M. Szyniszewski, O. Lunt, and A. Pal, *Phys. Rev. B* **108**, 165126 (2023).

[66] O. Alberton, M. Buchhold, and S. Diehl, *Phys. Rev. Lett.* **126**, 170602 (2021).

[67] R. D. Soares, Y. Le Gal, and M. Schiró, *Phys. Rev. B* **111**, 064313 (2025).

[68] T. Botzung, S. Diehl, and M. Müller, *Phys. Rev. B* **104**, 184422 (2021).

[69] B. Nienhuis, *Phys. Rev. Lett.* **49**, 1062 (1982).

[70] R. J. Baxter, *Journal of Physics A: Mathematical and General* **19**, 2821 (1986).

[71] P. di Francesco, H. Saleur, and J. B. Zuber, *Journal of Statistical Physics* **49**, 57–79 (1987).

[72] M. T. Batchelor and H. W. J. Blöte, *Phys. Rev. Lett.* **61**, 138 (1988).

[73] H. W. J. Blöte and B. Nienhuis, *Journal of Physics A: Mathematical and General* **22**, 1415 (1989).

[74] J. L. Jacobsen, “Conformal field theory applied to loop models,” in *Polygons, Polyominoes and Polycubes*, edited by A. J. Guttmann (Springer Netherlands, Dordrecht, 2009) pp. 347–424.

[75] L. Grans-Samuelsson, R. Nivesvivat, J. L. Jacobsen, S. Ribault, and H. Saleur, *SciPost Phys.* **12**, 147 (2022).

[76] J. L. Jacobsen, R. Nivesvivat, and H. Saleur, *SciPost Phys.* **16**, 111 (2024).

[77] V. Gorbenko and B. Zan, *Journal of High Energy Physics* **2020** (2020), 10.1007/jhep10(2020)099.

[78] J. L. Jacobsen, S. Ribault, and H. Saleur, *SciPost Phys.* **14**, 092 (2023).

[79] J. L. Jacobsen and H. Saleur, *Journal of High Energy Physics* **2023** (2023), 10.1007/jhep12(2023)090.

[80] J. L. Jacobsen, N. Read, and H. Saleur, *Phys. Rev. Lett.* **90**, 090601 (2003).

[81] W. J. L. Buyers, R. M. Morra, R. L. Armstrong, M. J. Hogan, P. Gerlach, and K. Hirakawa, *Phys. Rev. Lett.* **56**, 371 (1986).

[82] J. P. Renard, M. Verdaguer, L. P. Regnault, W. A. C. Erkelens, J. Rossat-Mignod, and W. G. Stirling, *Europhysics Letters* **3**, 945 (1987).

[83] P. Sompé, S. Hirthe, D. Bourgund, T. Chalopin, J. Bibo, J. Koepsell, P. Bojović, R. Verresen, F. Pollmann, G. Salomon, C. Gross, T. A. Hilker, and I. Bloch, *Nature* **606**, 484 (2022).

[84] C. Edmunds, E. Rico, I. Arrazola, G. Brennen, M. Meth, R. Blatt, and M. Ringbauer, *PRX Quantum* **6**, 020349 (2025).

[85] We use integer spin $S = 1$ so that the $\theta = 2\pi S$ topological term does not change the physics in the bulk.

[86] I. Affleck, in *Fields, Strings and Critical Phenomena*, Les Houches Summer School of Theoretical Physics, Vol. Session XLIX, edited by E. Brézin and J. Zinn-Justin (North-Holland, Amsterdam, 1990) pp. 563–640.

[87] J. L. Cardy, *Journal of Physics A: Mathematical and General* **17**, L385 (1984).

[88] Strictly speaking, depending on the value of $\text{Arg}[v]$ another primary could have been the state with the lowest real part of the energy, but this does not happen for the value of v we found.

[89] F. Minganti, D. Huybrechts, C. Elouard, F. Nori, and I. I. Arkhipov, *Phys. Rev. A* **106**, 042210 (2022).

[90] Y. Ashida, Z. Gong, and M. Ueda,

Advances in Physics **69**, 249 (2020), <https://doi.org/10.1080/00018732.2021.1876991>.

[91] F. Roccati, G. M. Palma, F. Ciccarello, and F. Bagarello, Open Systems & Information Dynamics **29**, 2250004 (2022), <https://doi.org/10.1142/S1230161222500044>.

[92] W. Bernreuther and F. J. Wegner, Phys. Rev. Lett. **57**, 1383 (1986).

[93] L. Burgelman, L. Devos, B. Vanhecke, F. Verstraete, and L. Vanderstraeten, Phys. Rev. E **107**, 014117 (2023).

[94] M. Fava, L. Piroli, T. Swann, D. Bernard, and A. Nahum, Phys. Rev. X **13**, 041045 (2023).

[95] P. Cvitanovic, *Group Theory: Birdtracks, Lie's, and Exceptional Groups* (Princeton University Press, 2008).

[96] P.-Y. Chang, J.-S. You, X. Wen, and S. Ryu, Phys. Rev. Res. **2**, 033069 (2020).

[97] C. H. Lee, Phys. Rev. Lett. **128**, 010402 (2022).

[98] Y.-B. Guo, Y.-C. Yu, R.-Z. Huang, L.-P. Yang, R.-Z. Chi, H.-J. Liao, and T. Xiang, Journal of Physics: Condensed Matter **33**, 475502 (2021).

[99] W.-T. Xue and C. H. Lee, “Topologically protected non-hermitian super-volume-law entanglement,” (2024).

[100] S. Ryu and J. Yoon, Phys. Rev. Lett. **130**, 241602 (2023).

[101] C.-T. Hsieh and P.-Y. Chang, SciPost Phys. Core **6**, 062 (2023).

[102] M. Fossati, F. Ares, and P. Calabrese, Phys. Rev. B **107**, 205153 (2023).

[103] P. Calabrese and J. Cardy, Journal of Statistical Mechanics: Theory and Experiment **2004**, P06002 (2004).

[104] C. Holzhey, F. Larsen, and F. Wilczek, Nuclear Physics B **424**, 443 (1994).

[105] G. Vidal, J. I. Latorre, E. Rico, and A. Kitaev, Phys. Rev. Lett. **90**, 227902 (2003).

[106] P. Calabrese, M. Campostrini, F. Essler, and B. Nienhuis, Phys. Rev. Lett. **104**, 095701 (2010).

[107] S. R. White, Phys. Rev. Lett. **69**, 2863 (1992).

[108] M. Fishman, S. R. White, and E. M. Stoudenmire, SciPost Phys. Codebases, 4 (2022).

[109] H. W. J. Blöte, J. L. Cardy, and M. P. Nightingale, Phys. Rev. Lett. **56**, 742 (1986).

[110] P. Di Francesco, P. Mathieu, and D. Sénéchal, *Conformal Field Theory* (Springer New York, 1997).

[111] J. Cardy, “Conformal field theory and statistical mechanics,” (2008).

End Matter

Optimization procedure.— We use a gradient descent algorithm to locate the finite-size critical point in the parameter space (J_2, K) with the fastest finite-size convergence. We do so by matching the thermal and $\ell = 1$ watermelon scaling dimensions in the spin chain spectrum with their predicted values. To extract these scaling dimensions, we compare the momentum k and total spin S of the eigenstates to the known symmetries of the CCFT primaries, see Refs. [77, 78]. We will use $E_{k,S}^\nu$ to denote the eigenenergies and $\nu \in \mathbb{Z}^+$ to index the states in order of increasing real energy. The CCFT vacuum is a translationally-invariant singlet and naturally corresponds to the Haldane ground state with energy $E_g = E_{k=0,S=0}^0$. The thermal operator is a singlet, so it corresponds to $E_{k=0,S=0}^1$. The $\ell = 1$ WM is the $O(3)$ vector operator and has momentum $k = \pi$ since this is an antiferromagnetic model: it thus corresponds to $E_{k=\pi,S=1}^0$. Finally, the velocity

$$v = \frac{L}{2\pi} (E_{k=\pi+2\pi/L,S=1}^0 - E_{k=\pi,S=1}^0) \quad (10)$$

can be inferred from the first descendant state of the $\ell = 1$ WM at $k = \pi + 2\pi/L$. The resulting $\ell = 1$ WM and thermal scaling dimensions are respectively given by

$$\Delta_{\ell=1}^{\text{calc}} = \frac{E_{k=\pi,S=1}^0 - E_g}{2\pi v/L}, \text{ and } \Delta_\epsilon^{\text{calc}} = \frac{E_{k=0,S=0}^1 - E_g}{2\pi v/L}. \quad (11)$$

Using the calculated scaling dimensions from exact diagonalization, we can now locate the finite-size critical point with fastest convergence by searching for the minima of the cost function $f(J_2, K) = |R_1| + w|R_2|$ through

gradient descent, where

$$R_1 = \frac{\Delta_{\ell=1}}{\Delta_\epsilon} - \frac{\Delta_{\ell=1}^{\text{calc}}}{\Delta_\epsilon^{\text{calc}}}, \quad R_2 = \frac{\Delta_\epsilon}{\Delta_\epsilon^{\text{calc}}} - 1. \quad (12)$$

and $w = 0.2$ is a feature scaling weight which we found to help the gradient descent algorithm. We emphasize that the two-parameter optimization over J_2 and K is used solely to improve finite-size numerics, and only a single complex tuning parameter should be needed to realize the CCFT in the thermodynamic limit.

Identification of watermelon operators in the spectrum.—We now discuss the identification of ℓ -leg watermelon operators in our spectrum for $\ell = 1, 2, 3, 4$. For each ℓ value, we find the decomposition into $O(N)$ irreducible representations in Ref. [78], and we then specialize to $N = 3$ (for a reference on the multiplicity of Young tableaux of $O(N)$, see [95]). We find perfect agreement with the multiplicity we observe in our numerics (see clusters labeled A, B, C, D) in Fig. 3c). For $\ell = 1$, Ref. [78] gives the $O(N)$ irreducible representation [1] (using row-length notation for Young tableaux), i.e. an $S = 1$ state in the case of $N = 3$. This is the $O(N)$ vector field. We confirm this numerically (point A). For $\ell = 2$, Ref. [78] gives [2], i.e. an $S = 2$ state, which we confirm numerically (point B). This is the symmetric traceless rank-2 tensor. For $\ell = 3$, Ref. [78] gives [3] + [111], which for $N = 3$ specializes to $3 \oplus 0$, i.e. a spin-3 and a singlet. Microscopically, the singlet operator is identified with $\mathbf{S}_i \cdot (\mathbf{S}_j \times \mathbf{S}_k)$. We confirm the presence of both the spin 0 (point C0) and the spin 3 (point C3) states. For $\ell = 4$, Ref. [78] gives [4] + [2] + [0] + [22] + [211]. For $O(3)$,

the multiplicity of [22] and [211] is zero (see e.g. Table 10.3 and 10.4 of [95]), leaving only $4 \oplus 2 \oplus 0$. The singlet state is the previously discussed loop crossing operator that appears in the action and is weakly irrelevant. We have confirmed the presence of a $S = 4$, $S = 2$ and $S = 0$ state close to the predicted $\ell = 4$ WM scaling dimension (see points D0, D2, and D4). We summarize all the calculated scaling dimensions in Fig. 3(d).

Entanglement entropy and central charge.—We provide further evidence of the CCFT by calculating the central charge through two complementary approaches: the entanglement entropy and the finite-size scaling of the ground state energy.

For non-Hermitian Hamiltonians, the generalized entanglement entropy is a complex quantity [39, 53, 55, 96–102]. It is defined using the biorthonormal ground-state density matrix $\rho = |\psi_R\rangle\langle\psi_L|$, where $|\psi_R\rangle$ and $\langle\psi_L|$ denote the right and left ground states satisfying $H|\psi_R\rangle = E_g|\psi_R\rangle$ and $\langle\psi_L|H = \langle\psi_L|E_g$. The entanglement entropy $S(l) = \text{Tr}_A(\rho_A \log \rho_A)$ follows from the reduced density matrix $\rho_A = \text{Tr}_B(\rho)$, obtained by tracing out a subsystem B of length $L - l$. At criticality, $S(l)$ displays the characteristic logarithmic scaling controlled by the central charge c ,

$$S(l) = \frac{c}{3} \log \left(\frac{L}{\pi} \sin \frac{\pi l}{L} \right) + s_0, \quad (13)$$

where s_0 is a non-universal constant and c may be complex [39, 55, 103–106]. The numerical results, calculated using the density matrix renormalization group (DMRG) on a length $L = 14$ chain with periodic boundary conditions [107, 108], are presented in Figs. 5(a)–(b) and display agreement with the logarithmic scaling form. The optimal fit on the interval $l \in [2, 12]$ yields $c = 1.529 - 0.161i$ within 2% of the predicted value $c_+ = 1.51 - 0.158i$.

The central charge c also governs the scaling of the ground-state energy as

$$E_g = e_\infty L - \frac{\pi v c}{6L} + O(L^{-2}), \quad (14)$$

where e_∞ denotes the non-universal bulk energy density and v is the velocity [109–111]. In Fig. 5(c)–(d), we plot E_g/L and fit the data using e_∞ as a free parameter. Here, we have used the value of c obtained from the entanglement entropy and the velocity determined from the spectrum (see Eq. (10)). The agreement indicates that the finite-size scaling is consistent with the CCFT prediction.

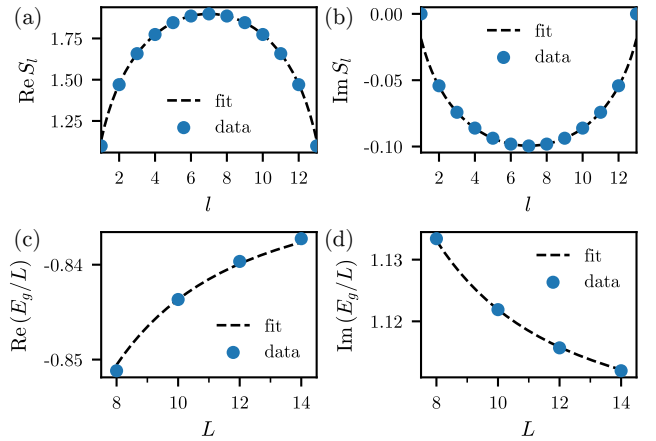


FIG. 5. (a)–(b) Real and imaginary parts of the complex entanglement entropy S_l for different subsystem sizes l at the CCFT. The dashed line indicates the fit to the logarithmic scaling expected at criticality [see Eq. (13)], which estimates the central charge to be $c = 1.529 - 0.161i$. (c)–(d) Real and imaginary parts of the ground-state energy density E_g/L and fit to $E_g/L = e_\infty - \pi v c/(6L^2)$, where e_∞ is a fitting parameter, c is determined from the entanglement entropy [see panels (a)–(b)], and v is obtained from the energy spectrum [see Eq. (10)].